Tuning Conversion Efficiency in Metallo Endohedral Fullerene-Based Organic Photovoltaic Devices

By *Russel B. Ross, Claudia M. Cardona, Francis B. Swain, Dirk M. Guldi, Shankara G. Sankaranarayanan, Edward Van Keuren, Brian C. Holloway,* and *Martin Drees**

Here the influence that 1-(3-hexoxycarbonyl)propyl-1-phenyl-[6,6]-$Lu_3N@C_{81}$, $Lu_3N@C_{80}$–PCBH, a novel acceptor material, has on active layer morphology and the performance of organic photovoltaic (OPV) devices using this material is reported. Polymer/fullerene blend films with poly(3-hexylthiophene), P3HT, donor material and $Lu_3N@C_{80}$–PCBH acceptor material are studied using absorption spectroscopy, grazing incident X-ray diffraction and photocurrent spectra of photovoltaic devices. Due to a smaller molecular orbital offset the OPV devices built with $Lu_3N@C_{80}$–PCBH display increased open circuit voltage over empty cage fullerene acceptors. The photovoltaic performance of these metallo endohedral fullerene blend films is found to be highly impacted by the fullerene loading. The results indicate that the optimized blend ratio in a P3HT matrix differs from a molecular equivalent of an optimized P3HT/[6,6]-phenyl-C_{61}-butyric methyl ester, C_{60}–PCBM, active layer, and this is related to the physical differences of the C_{80} fullerene. The influence that active layer annealing has on the OPV performance is further evaluated. Through properly matching the film processing and the donor/acceptor ratio, devices with power conversion efficiency greater than 4% are demonstrated.

1. Introduction

In recent years organic photovoltaics, OPVs, have gained an increasing amount of attention for their potential use as low-cost solar energy conversion devices. However, the power conversion efficiency of OPV technologies remains relatively low compared to other photovoltaic technologies; there have only been a few reports of OPV device efficiencies over 5%.[1,2] This is in part due to energy level offset between the available donor and acceptor materials.[3–7] When a photon of light is absorbed in donor systems like poly(3-hexylthiophene), P3HT, an exciton, a bound charge pair, is created which spans the donor's highest occupied molecular orbital, HOMO, and lowest unoccupied molecular orbital, LUMO. In bulk-heterojunction OPVs an acceptor material is mixed with a donor material to dissociate the excitons via a transfer of the excited state electrons from the LUMO of the donor to the lower energy LUMO of the acceptor.[8,9] Novel acceptor materials with LUMO energies closer to that of the donor, such as the derivatives of metallo endohedral fullerenes $M_3N@C_{80}$ (M = Sc, Y, Gd, Tb, Dy, Ho, Er, Tm, Lu), offer the possibility of dramatically increasing OPV power conversion efficiency, PCE, by utilizing more of the energy associated with the exciton.

While devices have been fabricated out of several $M_3N@C_{80}$ species, $Lu_3N@C_{80}$ was used for all devices described here. $Lu_3N@C_{80}$ was chosen because it has one of the highest LUMO energies among the $M_3N@C_{80}$ fullerenes, with a 280 mV advantage over C_{60} or C_{70}. By functionalizing this fullerene to 1-(3-hexoxycarbonyl)propyl-1-phenyl-[6,6]-$Lu_3N@C_{81}$, $Lu_3N@C_{80}$–PCBH, the derivative retains the 280 mV LUMO advantage over the widely used [6,6]-phenyl-C_{61}-butyric methyl ester, C_{60}-PCBM, with similar solubility and electron mobility.[10] The LUMO advantage of $Lu_3N@C_{80}$–PCBH manifests itself in the OPV device's higher open circuit voltage, V_{oc}.[3] We have reported OPV devices fabricated with the $Lu_3N@C_{80}$–PCBH acceptor using similar processing techniques as those employed for P3HT/C_{60}-PCBM system.[10] The previous report established that the 280 mV V_{oc} advantage is attainable, and that metallo endohedral fullerene acceptor materials set a direct path to higher PCE in a wide range of donor systems.[10] However, the previous work did not report on the significant physical differences of the $Lu_3N@C_{80}$–PCBH acceptor compared to C_{60}-PCBM. Here we demonstrate how molecular weight, fullerene size, and excited state lifetime affect the optimal performance of the OPV blend active layer.[10]

[*] Dr. M. Drees, Dr. C. M. Cardona, F. B. Swain, Dr. B. C. Holloway
Luna Innovations Incorporated
521 Bridge Street
Danville, VA 24541 (USA)
E-mail: dreesm@lunainnovations.com
R. B. Ross, Prof. E. Van Keuren
Georgetown University
37th and O St. NW, Washington, DC 20057 (USA)
Prof. D. M. Guldi, Dr. S. G. Sankaranarayanan
Interdisciplinary Center for Molecular Materials (ICMM)
Friedrich-Alexander-Universität Erlangen-Nürnberg
Egerlandstr. 3 91058 Erlangen (Germany)

DOI: 10.1002/adfm.200900214

This paper focuses on formation of the polymer/fullerene network, the most important aspect for high OPV performance. Through utilization of grazing incident x-ray diffraction (GIXRD), absorption spectra, and device data we conclude that the polymer-acceptor interactions of the $Lu_3N@C_{80}$–PCBH acceptor molecules are similar to that of C_{60}-PCBM and more importantly, the relative size of the C_{80} acceptor molecule influences the blend ratio needed to produce a high PCE device. By optimizing device construction parameters, P3HT/$Lu_3N@C_{80}$–PCBH devices having PCE >4% are achieved under AM1.5G solar simulation conditions, which is a consistently higher PCE than our optimized P3HT/C_{60}-PCBM reference devices (PCE = 3.4%).

2. Results and Discussion

The active layer of a bulk-heterojunction OPV device is a composite system made of two components: the first is the polymer donor which absorbs light and acts as a p-type semiconductor for hole transport to the anode. The second component is the fullerene acceptor which acts as an n-type semiconductor that accepts the excited state electrons from the donor polymer's LUMO and facilitates the transport of electrons for collection at the cathode.[11] In addition, the acceptor can also contribute to the photocurrent by transferring an excited state hole from its HOMO level to the donor. Blending of the polymer and fullerene into a bulk-heterojunction structure enhances the dissociation of excited state charge carriers by increasing the interfacial area between the donor and acceptor phases.

There are a number of techniques and architectures associated with the production of OPV devices. Common methods for active layer deposition include spray coating, drop casting, doctor blading, and spin casting. Although all of these techniques have shown great promise in device production, spin casting was chosen for this study because both the film thickness and the film's solidification time are easily altered and reproduced; this allows for a direct comparison with a majority of the OPV devices that have been reported in the literature.[12,13]

The efficiency with which charge carriers are generated, separated, and transported in the active layer is highly dependent upon the order of the P3HT phase and the overall morphology of the bulk-heterojunction structure which forms during solidification of a blend solution.[11,14,15] This junction will be affected by the ratio of the polymer donor and fullerene acceptor. $Lu_3N@C_{80}$–PCBH acceptor molecules have a molecular weight that is 93% greater than C_{60}-PCBM and they take up an expected 45% more volume than C_{60}-PCBM.[16] Here blend ratios are described in weight percentages of fullerene to total dry blend weight. The optimal blend ratio for P3HT/C_{60}-PCBM was found to be 44 wt% in this study. Using the molecular weight difference between C_{60}-PCBM and $Lu_3N@C_{80}$–PCBH, a 61 wt% of $Lu_3N@C_{80}$–PCBH would be required to achieve a molecular equivalent for a P3HT/$Lu_3N@C_{80}$–PCBH blend ratio. However, this calculated molecular equivalent does not take into account the volume difference of the $Lu_3N@C_{80}$–PCBH molecule, its molecular interactions, or the acceptor's excited state dynamics.

To evaluate the influence the fullerene has on the bulk-heterojunction structure, a series of films with varying $Lu_3N@C_{80}$–PCBH weight ratios were spin cast from blend solutions of donor, P3HT, and acceptor, $Lu_3N@C_{80}$–PCBH, solvated by 1,2-dichlorobenzene. After solidification, these films were annealed for one minute at 130 °C in an inert argon atmosphere to reduce any inhomogeneity induced by the drying process. Through the use of GIXRD and absorption spectra the overall order of the P3HT polymer phase is identified and used to optimize the blending ratio for P3HT/$Lu_3N@C_{80}$–PCBH OPV devices.

The GIXRD spectra of the polymer and fullerene phases in blend films of P3HT and $Lu_3N@C_{80}$–PCBH on low-noise quartz substrates can be seen in Figure 1a, normalized to the P3HT (100) peak at 2θ∼5.3°. The (100) peak of the P3HT has been documented as the planar separation of thiophene backbones parallel to the quartz substrate's surface.[17,18] Three films are shown at 0, 33, and 50 wt% fullerene loading. There is a concentration dependent halo which has been assigned to the $Lu_3N@C_{80}$–PCBH phase domains and is centered at 2θ∼8.4°. The mean fullerene separation spacing of 1.1 nm is calculated from the randomly oriented halo. This value matches well with

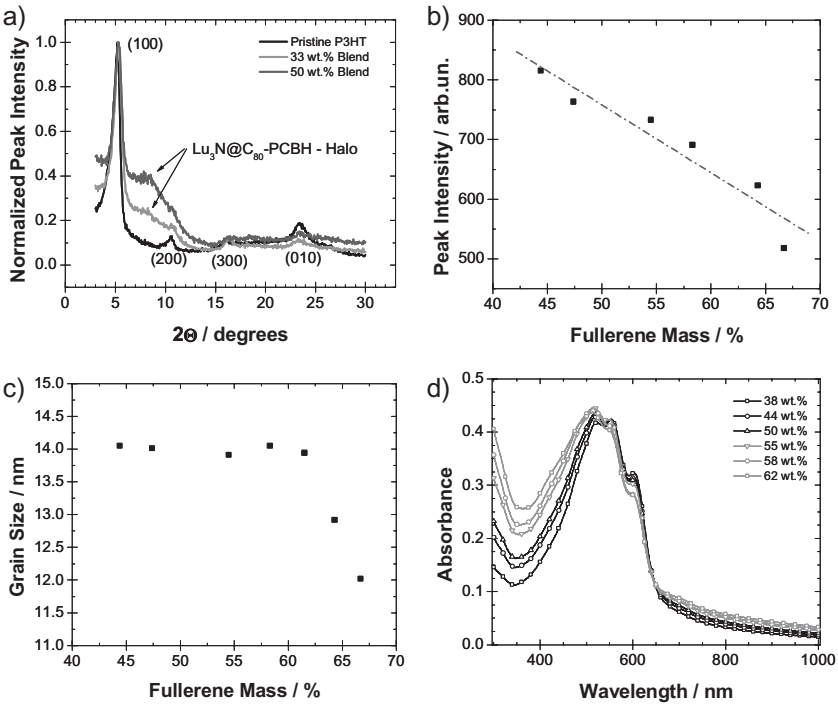

Figure 1. a) Identification of P3HT and $Lu_3N@C_{80}$–PCBH with using normalized GIXRD diffraction pattern for blend films at 0, 33, and 50 wt%, b) the influence $Lu_3N@C_{80}$–PCBH loading has on P3HT's (100) diffraction peak intensity and c) P3HT vertical grain size. Panel d) displays the blend film absorption spectra dependence on $Lu_3N@C_{80}$–PCBH loading.

those reported by other groups for highly ordered close packed hexagonal lattice of metallo endohedral C_{80} fullerenes.[19] When comparing the pristine P3HT film to that of the P3HT/$Lu_3N@C_{80}$–PCBH composite films there is a reproducible shift in the P3HT's (100) peak, indicating a compacting of the average vertical separation by 0.1 ° or ~0.2 Å. A similar shift (not shown) was observed for P3HT/C_{60}-PCBM reference films. This slight peak shift is an indication of stronger interlayer interactions which are induced by the presence of fullerene in the P3HT matrix, and has been noted by others for the P3HT/C_{60}-PCBM composite system.[15] More importantly, the (100) P3HT peak height has also been documented as a measure of the overall P3HT film order.[18] In Figure 1b the relative (100) peak heights, corrected for the film thickness, are shown as a function of $Lu_3N@C_{80}$–PCBH content in the blended films. A consistent trend develops indicating that increases in $Lu_3N@C_{80}$–PCBH loading contribute to decreases in overall P3HT order. A similar effect has been witness by others for the P3HT/C_{60}-PCBM system.[20] The polymer grain sizes calculated using Scherrer's relation indicate that the polymer grains remain unchanged for films with fullerene content up to 62 wt%, (Fig. 1c).[18,21] These P3HT grains surrounded by fullerene are the basic units that create the bulk-heterojunction structure, and this interface between the polymer phase and the fullerene phase is where charge carriers are dissociated. Recently, Shaw et al. showed the exciton diffusion length for P3HT to be ~8.5 nm.[22] Therefore, the radial distance of the ~14 nm P3HT domains is sufficient for full charge extraction at the donor/acceptor interface. Figure 1c shows that the films with fullerene loading above 62 wt% displayed decreasing polymer grain size which indicates an incorporation of fullerene into the polymer grains. This reduction in P3HT grain size and overall order is undesirable because it leads to an inefficient percolation network, which decreases the overall charge transport. Therefore, these GIXRD measurements establish an upper limit for the $Lu_3N@C_{80}$–PCBH content in the P3HT matrix at 62 wt%, which exceeds the calculated molecular equivalent weight ratio described above. The GIXRD also indicates that for weight ratios less than the 62 wt%, the polymer forms similar sized grains, but the overall order of the P3HT declines with increased fullerene loading (Fig. 1b). This interruption in the overall P3HT order is expected to blue shift the absorption spectra of the films and decrease the photon harvesting efficiency of the bulk-heterojunction.

The absorption spectra of the blend films shown in Figure 1d indicate that increases in the films' fullerene concentration does impact the overall film absorption. The presence of $Lu_3N@C_{80}$–PCBH in the spectra is identified by the increase in ultra-violet absorption (300–400 nm). The spectra exhibit a maxima in the visible region which blue shifts from 550 nm to 518 nm with increasing fullerene content. This blue shift in absorption is consistent with GIXRD data and previous literature, which found that blue shifts in P3HT absorption are due to lowering of P3HT's overall order.[13,23] The blend films also display P3HT's vibronic shoulders at 550 nm and 602 nm which have been attributed to polymer/polymer intermolecular interactions.[24] However, there is discontinuity between the vibronic patterns in the spectra of blend ratios 55 wt% and 58 wt%. Although GIXRD spectra of the P3HT's (100) peak height suggests a steady decrease in polymer order with increasing fullerene loading, this discontinuity in the absorption spectra is correlated to the onset of the fullerene's disruption of the highly ordered polymer domains and is in this respect consistent with the grain sizes measured with GIXRD. These results from both the GIXRD and absorption measurements clearly indicate a threshold does exist for $Lu_3N@C_{80}$–PCBH content in the P3HT matrix, above which the ordering of the P3HT is significantly interrupted. However, the interpretation of the vibronic shoulder discontinuity presented in the absorption spectra indicates that the ordering threshold is better placed at 55 wt% for the P3HT/$Lu_3N@C_{80}$–PCBH system. This is still well below the expected 61 wt% for a molecular equivalent of a P3HT/C_{60}-PCBM optimized composite film.

To relate the observed morphology changes to OPV device performance, OPV devices were built using the P3HT/$Lu_3N@C_{80}$–PCBH blends with similar processing conditions as those used for the GIXRD and absorption analysis. These blend films were spin cast onto glass/ITO/PEDOT-PSS substrates, and a LiF/Al top cathode was deposited with a post-production anneal for 1 min at 130 °C. In a comprehensive evaluation of common electrode interface materials it was found that an ITO/PEDOT-PSS anode and a sequentially deposited LiF/Al cathode provided the best photocurrent and fill factors. For consistency single-layer devices were used for this study.

As shown in Figure 1d, the blend films' absorption in the visible region is dominated by that of P3HT. It is reasonable to expect that the blend films will harvest photons similarly. Differences in the blend films' performances can therefore be associated with differences in excited state dissociation and charge transport properties influenced by the bulk morphology. Using photocurrent spectra to establish each of the P3HT/$Lu_3N@C_{80}$–PCBH blends' external quantum efficiency, EQE, the efficiency at which one photon at a given energy is converted to an electron in the external circuit, we find significant differences among the various fullerene loadings (see Fig. 2a and b). The relative intensity of the EQE indicated an optimization window for the blend ratio between 44 wt% and 55 wt%. This maximizing effect of the EQE is a direct example of the interplay between the percolation and interpenetration of both the polymer and fullerene phases that maximizes both charge transport and charge separation.

Additional trends are apparent in the EQE data for fullerene ratios larger and smaller than the optimal 50 wt% blend. In Figure 2a the 64 wt% device exhibits a reduction in overall photon conversion, and its normalized spectra in Figure 2b exhibits a peak narrowing in photon conversion. This demonstrates how the overloading of fullerene disrupts the polymer phase, which negatively influences the charge transport and limits the photocurrent. Thus the EQE data corroborates the GIXRD and absorption data discussed above.

Not only are there shifts observed in the EQE spectra due to polymer phase order, but also there are shifts in the UV-region (300–400 nm) which indicate that the fullerene loading affects hole transfer from the fullerene to the polymer. In Figure 2b there is a noticeable blue shift of the EQE in the UV region. This blue shift develops with a decrease in fullerene loading, contrary to the blue shift seen at 600 nm. It has been shown with P3HT/C_{60}-PCBM composites that the photo-excited fullerene contributes to the photocurrent in this region of the spectra through a hole transfer from the fullerene's HOMO to the polymer's HOMO.[25]

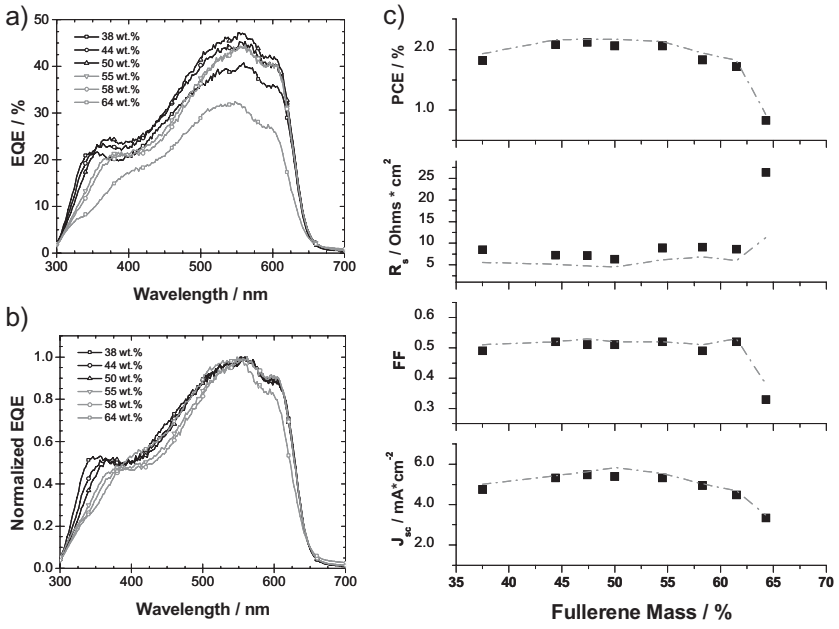

Figure 2. a) Displays external quantum efficiency, EQE, spectra for P3HT/$Lu_3N@C_{80}$–PCBH solar cells with varying fullerene loading and b) normalized to peak intensity. Device characteristics under solar simulated illumination are present in panel c). Filled squares depict average solar cell device characteristics for six devices with varying amounts of $Lu_3N@C_{80}$–PCBH (all devices have active-layer thickness ~85 nm). Grey dashed line indicates maximum PCE, minimum series resistance (R_s), maximum Fill Factor (FF), and maximum Short Circuit Current (J_{sc}) for this series of devices.

As the fullerene loading is decreased, the overall composite takes on a shape closer to the pure P3HT absorption; thereby reducing the absorption in the 300–400 nm region and also the number of absorbed photons that contribute to the photocurrent in the UV-region of the spectrum. The EQE spectra are in opposition to this expected trend shown in Figure 2b. We attribute this result to the metallo endohedral fullerene's excited state lifetime. Transient absorption measurements of $Lu_3N@C_{80}$–PCBH have shown that the singlet excited state lifetime is 62 times shorter than C_{60}-PCBM (1800 ps).[26] Increases of $Lu_3N@C_{80}$–PCBH loading in the P3HT matrix lead to larger fullerene domains, similar to what is observed for C_{60}-PCBM,[27] and therefore on average the excitons created in the fullerene domains have to traverse a larger distance to reach a donor/acceptor interface. This longer distance to a donor/acceptor interface combined with a short excited state lifetime means more excitons will recombine before reaching the interface and subsequently decrease the fullerene's contribution to the photocurrent.

Analysis of a series of devices at each blend ratio under an AM1.5G filtered solar simulator found that the PCE correlated with the EQE measurement, as shown in Figure 2c. The improved morphology of the 50 wt% blend ratio indicated by GIXRD and film absorption was further confirmed in these devices by measuring average minimum series resistance of 6.3 Ω cm^2 for the devices in the dark at 2 V forward bias. The maximum PCE of the devices is shown to be dominated by the photocurrent which is more sensitive to carrier mobility than V_{oc} or fill factor (FF).[28] These findings identify that there is a need for a balanced network in the active layer. The maximum in the EQE spectra shows that the balance between high order in P3HT for efficient hole transport and percolation of the fullerene network for efficient electron transport is achieved at 50 wt% $Lu_3N@C_{80}$–PCBH loading The presented differences in the optimal fullerene loading found at 50 wt% and the molecular equivalent loading calculated to be at 61 wt% demonstrate the impact the fullerene volume has on the percolation network, but does not account for the estimated 45% volume difference. This discrepancy in total volume of fullerene is attributed to the packing differences of the functionalized C_{80} verses C_{60}-PCBM; as well as the fullerene's intermolecular interactions, and excited state dynamics such as lifetimes and charge carrier mobility that play a role in balancing the charge dissociation and transport properties of the active layer.

Techniques such as thermal annealing of P3HT composite films have been shown to increase device efficiency through morphology modification and improvement in active layer/electrode contact.[15,29,30] Studies have also shown that OPV devices perform differently if annealed before or after the deposition of the metal cathode, and that these increases in performance are highly dependent on the blend film's dry time.[13,31–33] To study the influence of annealing on P3HT/$Lu_3N@C_{80}$–PCBH devices, blend films at 50 wt.% were subjected to a prolonged annealing at 130 °C for 3 min before or after cathode deposition. The absorption spectra shown in Figure 3a are of two films, one annealed before and one annealed after electrode deposition. The overlapping absorption spectra of these two films demonstrate that the films have similar bulk morphology. However, by integrating both EQE spectra the device annealed post-electrode deposition has a 1.77 mA cm^{-2} larger photocurrent (results shown in Fig. 3b). The *JV* characteristics shown in Figure 3c demonstrate that the device annealed after

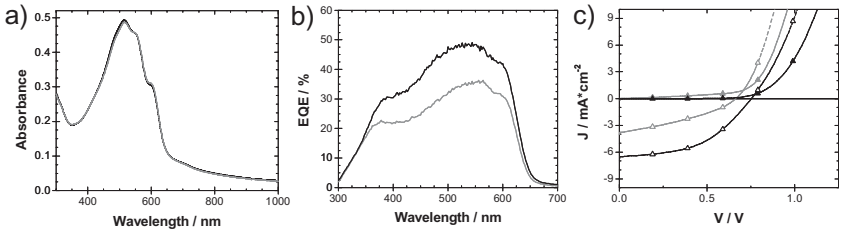

Figure 3. a) Absorption of 0.50 wt% P3HT/$Lu_3N@C_{80}$–PCBH films with a pre-production anneal (grey) and a post-production anneal (black). b) The EQE spectra of the same films. c) The current-voltage characteristics of the two films in the dark (filled triangles) and under solar simulated illumination (open triangles).

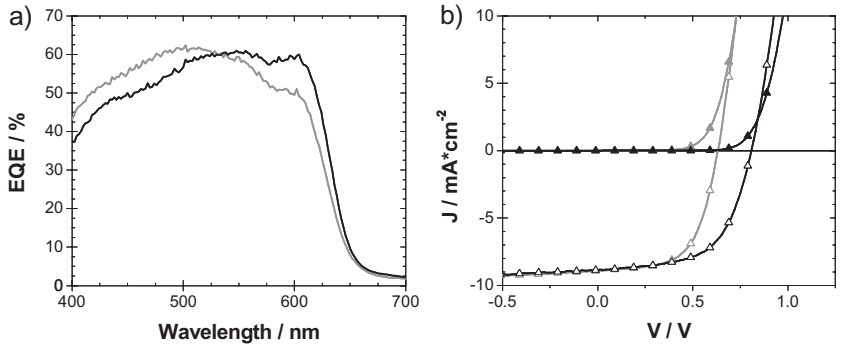

Figure 4. a) The EQE of P3HT/$Lu_3N@C_{80}$–PCBH (black) and P3HT/C_{60}-PCBM (grey) blend devices. b) Current-voltage characteristics of P3HT/$Lu_3N@C_{80}$–PCBH and P3HT/C_{60}-PCBM blend devices. Solid triangles indicate the dark *JV* curves and open triangles indicate the devices' *JV* curve under solar simulated illumination.

electrode deposition not only has higher short circuit current (J_{sc}), but also higher V_{oc} and FF. Since both films only differ in the annealing step and display similar bulk morphology the higher overall performance of the post-production annealed film is attributed to an enhanced contact between the active layer and the device's anode and cathode. It is worth mentioning here that the P3HT/$Lu_3N@C_{80}$–PCBH devices produced during this study did not display PCE values greater than 2% unless the active-layer underwent some form of annealing.

Similar work for P3HT/C_{60}-PCBM devices have shown that slowing the dry-time of the blend film induces highly ordered P3HT domains but also increases surface roughness that may interfere with electrode contact.[13,33] In this part of the study dry times were held to within 10 min after the 30 s spin coating of the active-layer by placing the wet film in a closed container. Li et al. reported on the P3HT/C_{60}-PCBM that, when the film dry time is extended, a low-temperature, 110 °C, anneal step before the electrode deposition leads to higher device performances through flatter surface morphology and reduces the level of residual solvent in the blend film.[13,33] Therefore, a combination of pre-production anneal to improve the surface morphology and a post-production anneal to improve the electrode contact were investigated to further improve device performance. A series of blend devices were built with various pre- and post-production anneals and optimized for thickness by changing the speed and duration of the spin coating process. An optimized P3HT/$Lu_3N@C_{80}$–PCBH device produced in this manner is shown in Figure 4a and b, with an improved performance of PCE = 4.24% (V_{oc} = 810 mV, J_{sc} = 8.85 mA cm^{-2}, and FF = 59%). For comparison, a device using the same architecture and optimized with a C_{60}-PCBM acceptor is overlaid (V_{oc} = 630 mV, J_{sc} = 8.9 mAcm^{-2}, and FF = 61%) in Figure 4. By annealing the P3HT/$Lu_3N@C_{80}$–PCBH device for a longer period (10 min) at relatively low temperatures (110 °C) before the LiF/Al is deposited, the film is allowed to further order and flatten without the constraint of a metal electrode, while the brief thirty second higher temperature (140 °C) post-production anneal aids to improve the cathode contact, thus increasing the overall performance of the device. The enhanced performance of the $Lu_3N@C_{80}$–PCBH devices is due to the improved open circuit voltage while matching the short circuit current and fill factor of the C_{60}-PCBM reference device.

3. Concluding Remarks

The advantage of higher LUMO levels in metallo endohedral fullerene derivatives such as $Lu_3N@C_{80}$–PCBH offers a direct pathway to greater efficiency OPV devices by reducing the energy loss of the photo-excited electrons. Through comparative analysis of the film absorption and x-ray diffraction we ascertained an optimal blend ratio of P3HT and $Lu_3N@C_{80}$–PCBH of 50 wt% fullerene loading, which is not the one-to-one molecular equivalent weight ratio of a typical C_{60}-PCBM system. The difference in the optimal blend ratio is due to the increased size of the $Lu_3N@C_{80}$–PCBH, thereby effectively reducing the amount of fullerene needed for efficient charge transport to occur. GIXRD results also indicate that $Lu_3N@C_{80}$–PCBH promotes phase segregation of P3HT similar to C_{60}-PCBM, and increases interlayer interactions in the P3HT matrix. Analysis of device performance as a function of blend ratio revealed that $Lu_3N@C_{80}$–PCBH requires a finer network to harvest the excitons on the fullerenes due to the shorter singlet excited state lifetime in these molecules. Further a post-production anneal is required for efficient devices; by performing a combination of pre and post-production anneal on P3HT/$Lu_3N@C_{80}$–PCBH devices, we produced devices with higher PCE values than our P3HT/C_{60}-PCBM reference devices. These results clearly demonstrate the superior performance of a donor/acceptor system that has a smaller LUMO energy offset compared to the commonly used P3HT/C_{60}-PCBM system.

4. Experimental Details

Low noise polished quartz substrates were acquired from Dug Out Supplies for the GIXRD measurements. The blend films used for GIXRD were spin cast at 500 rpm for 30 s in an inert argon atmosphere. The 1-D GIXRD spectra were measured using a Philips X'Pert PRO MRD HR X-Ray Diffraction System with Cu Kα (1.5405 Å) source. Film thicknesses were measured on a Veeco CP-II AFM, and all UV/Vis absorption spectra of the blend films and devices were measured on a Perkin-Elmer Lamdba-20.

OPV devices were fabricated on indium tin oxide (ITO) coated glass substrates (8-10 Ω/□, Delta Technologies, Limited). The substrates were cleaned by subsequent sonication for 15 minutes in detergent solution (Fl-70, Fisher Scientific), deionized water, acetone, and isopropanol. Substrates were dried in an N_2 stream and a 35 nm layer of PEDOT:PSS (Baytron P AI 4083, H.C. Stark) was spun in air. The substrates were baked in air for 10 min on a hot plate at 140 °C and immediately loaded into an Ar glove box (<0.1 ppm O_2 and <0.1 ppm H_2O) where all further processing took place.

The blends were prepared by first preparing a 20 mg mL^{-1} stock solution of P3HT (4002E, Rieke Metals) in 1,2-dichlorobenzene (Aldrich) that was allowed to stir for at least 24 h at 70 °C. This stock solution was added to the dry fullerene acceptors and the desired solution concentrations were achieved by adding 1,2-dichlorobenzene. The blend was heated at 70 °C and stirred to disperse the fullerene. The ~85 nm active layers were then spun at 800 rpm for 50 s, and the ~120 nm active layer devices were spun at 700 rpm for 30 s. The thermally deposited cathode was comprised of a 0.6 nm LiF layer, and a 95 nm Al layer both deposited at pressures $\leq 1 \times 10^{-6}$ mbar. The fabricated OPV devices were subjected to anneal procedures, as described in the text. Subsequent photo spectrum analysis

and device statistics were measured outside the glove box with the device in a sealed enclosure.

Device efficiencies were measured using a Keithley 236 source measure unit with illumination from a solar simulator (150W Newport-Oriel, Air Mass 1.5G filter) at 100 mWcm^{-2} referenced to a calibrated Si diode with KG3 filter (PV Measurement, Inc). The external quantum efficiency was measured using a Keithley 6485 picoammeter with monochromatic light focused on to an area smaller than the average device area, 0.12 cm^2, filtered by a CVI Spectral Products Monochromator with a 300 W Newport-Oriel Xeon lamp as the source and referenced to a calibrated Oriel Silicon model 71580 detector.

Acknowledgements

This material is based upon work supported by the Air Force Office of Scientific Research under Contract No. FA9550-06-C-0010. Any opinion, findings and conclusions or recommendations expressed in this material are those of the authors and do not necessarily reflect the views of the Air Force Office of Scientific Research. This material is also based upon work supported by the National Science Foundation under Grant No. 0348955 and Grant No. IIP-0740454. Additional thanks to the Cluster of Excellence ''Engineering of Advanced Materials'' and the Alexander von Humboldt Foundation for generous support (S.G.S.).

Received: February 2, 2009
Revised: March 6, 2009
Published online:

[1] J. Peet, J. Y. Kim, N. E. Coates, W. L. Ma, D. Moses, A. J. Heeger, G. C. Bazan, *Nat.Mater.* **2007**, *6*, 497.
[2] Y. Liang, Y. Wu, D. Feng, S.-T. Tsai, H.-J. Son, G. Li, L. Yu, *J. Am. Chem. Soc.* **2009**, *131*, 56.
[3] C. J. Brabec, A. Cravino, D. Meissner, N. S. Sariciftci, T. Fromherz, M. T. Rispens, L. Sanchez, J. C. Hummelen, *Adv. Funct. Mater.* **2001**, *11*, 374.
[4] C. J. Brabec, A. Cravino, D. Meissner, N. S. Sariciftci, M. T. Rispens, L. Sanchez, J. C. Hummelen, T. Fromherz, *Thin Solid Films* **2002**, *403–404*, 368.
[5] F. B. Kooistra, J. Knol, F. Kastenberg, L. M. Popescu, W. J. H. Verhees, J. M. Kroon, J. C. Hummelen, *Org. Lett.* **2007**, *9*, 551.
[6] M. Lenes, G. Wetzelaer, F. B. Kooistra, S. C. Veenstra, J. C. Hummelen, P. W. M. Blom, *Adv. Mater.* **2008**, *20*, 2116.
[7] M. C. Scharber, D. Wuhlbacher, M. Koppe, P. Denk, C. Waldauf, A. J. Heeger, C. L. Brabec, *Adv. Mater.* **2006**, *18*, 789.
[8] J. J. M. Halls, J. Cornil, D. A. dos Santos, R. Silbey, D. H. Hwang, A. B. Holmes, J. L. Bredas, R. H. Friend, *Phys. Rev. B* **1999**, *60*, 5721.
[9] C. J. Brabec, C. Winder, N. S. Sariciftci, J. C. Hummelen, A. Dhanabalan, P. A. van Hal, R. A. J. Janssen, *Adv. Funct. Mater.* **2002**, *12*, 709.
[10] R. B. Ross, C. M. Cardona, D. M. Guldi, S. G. Sankaranarayanan, M. Reese, N. Kopidakis, J. Peet, B. Walker, G. C. Bazan, E. Van Keuren, B. C. Holloway, M. Drees, *Nat. Mater.* **2009**, *8*, 208.
[11] G. Yu, J. Gao, J. C. Hummelen, F. Wudl, A. J. Heeger, *Science* **1995**, *270*, 1789.
[12] C. C. Chang, C. L. Pai, W. C. Chen, S. A. Jenekhe, *Thin Solid Films* **2005**, *479*, 254.
[13] G. Li, V. Shrotriya, J. S. Huang, Y. Yao, T. Moriarty, K. Emery, Y. Yang, *Nat. Mater.* **2005**, *4*, 864.
[14] H. Ohkita, S. Cook, Y. Astuti, W. Duffy, S. Tierney, W. Zhang, M. Heeney, L. McCulloch, J. Nelson, D. D. C. Bradley, J. R. Durrant, *J. Am. Chem. Soc.* **2008**, *130*, 3030.
[15] G. Li, Y. Yao, H. Yang, V. Shrotriya, G. Yang, Y. Yang, *Adv. Funct. Mater.* **2007**, *17*, 1636.
[16] B. W. Smith, D. E. Luzzi, Y. Achiba, *Chem. Phys. Lett.* **2000**, *331*, 137.
[17] T. J. Prosa, M. J. Winokur, J. Moulton, P. Smith, A. J. Heeger, *Macromolecules* **1992**, *25*, 4364.
[18] T. Erb, U. Zhokhavets, G. Gobsch, S. Raleva, B. Stuhn, P. Schilinsky, C. Waldauf, C. J. Brabec, *Adv. Funct. Mater.* **2005**, *15*, 1193.
[19] D. F. Leigh, C. Norenberg, D. Cattaneo, J. H. G. Owen, K. Porfyrakis, A. L. Bassi, A. Ardavan, G. A. D. Briggs, *Surf. Sci.* **2007**, *601*, 2750.
[20] M. Reyes-Reyes, R. Lopez-Sandoval, J. Arenas-Alatorre, R. Garibay-Alonso, D. L. Carroll, A. Lastras-Martinez, *Thin Solid Films* **2007**, *516*, 52.
[21] A. L. Patterson, *Phys. Rev.* **1939**, *56*, 978.
[22] A. R. I. D. W. S. Paul, E. Shaw, *Adv. Mater.* **2008**, *20*, 3516.
[23] V. Shrotriya, J. Ouyang, R. J. Tseng, G. Li, Y. Yang, *Chem. Phys. Lett.* **2005**, *411*, 138.
[24] M. Sundberg, O. Inganäs, S. Stafström, G. Gustafsson, B. Sjögren, *Solid State Commun.* **1989**, *71*, 435.
[25] W. Brütting, *Physics of Organic Semiconductors*, Wiley-VCH, Berlin **2005**, 441.
[26] R. B. Ross, C. M. Cardona, S. G. Sankaranarayanan, D. M. Guldi, E. Van Keuren, B. C. Holloway, M. Drees, unpublished.
[27] X. N. Yang, J. K. J. van Duren, R. A. J. Janssen, M. A. J. Michels, J. Loos, *Macromolecules* **2004**, *37*, 2151.
[28] V. D. Mihailetchi, J. Wildeman, P. W. M. Blom, *Phys. Rev. Lett.* **2005**, *94*, 4.
[29] V. D. Mihailetchi, H. X. Xie, B. de Boer, L. J. A. Koster, P. W. M. Blom, *Adv. Funct. Mater.* **2006**, *16*, 699.
[30] F. Padinger, R. S. Rittberger, N. S. Sariciftci, *Adv. Funct. Mater.* **2003**, *13*, 85.
[31] W. L. Ma, C. Y. Yang, X. Gong, K. Lee, A. J. Heeger, *Adv. Funct. Mater.* **2005**, *15*, 1617.
[32] G. Li, V. Shrotriya, Y. Yao, Y. Yang, *J. Appl. Phys.* **2005**, *98*, 5.
[33] G. Li, V. Shrotriya, Y. Yao, J. S. Huang, Y. Yang, *J. Mater. Chem.* **2007**, *17*, 3126.